Article

Development of Nanomedicine from Copper Mine Tailing Waste: A Pavement towards Circular Economy with Advanced Redox Nanotechnology

Amrita Banerjee [1,2], Ria Ghosh [3], Tapan Adhikari [4], Subhadipta Mukhopadhyay [1], Arpita Chattopadhyay [5,*] and Samir Kumar Pal [3,*]

[1] Department of Physics, Jadavpur University, Kolkata 700032, India
[2] Technical Research Centre, S. N. Bose National Centre for Basic Sciences, Block JD, Sector III, Salt Lake, Kolkata 700106, India
[3] Department of Chemical and Biological Sciences, S. N. Bose National Centre for Basic Sciences, Block JD, Sector 3, Salt Lake, Kolkata 700106, India
[4] Indian Institute of Soil Science Nabibagh, Bhopal 462038, India
[5] Department of Basic Science and Humanities, Techno International New Town, Block—DG 1/1, Action Area 1 New Town, Rajarhat, Kolkata 700156, India
[*] Correspondence: arpita.chattopadhyay@tict.edu.in (A.C.); skpal@bose.res.in (S.K.P.)

Abstract: Copper, the essential element required for the human body is well-known for its profound antibacterial properties, yet salts and oxides of copper metals in the copper mine tailings are reported to be a big burden in the modern era. Among other copper oxides, CuO, in particular, is known to have beneficial effects on humans, while its slight nanoengineering viz., surface functionalization of the nanometer-sized oxide is shown to make some paradigm shift using its inherent redox property. Here, we have synthesized nanometer-sized CuO nanoparticles and functionalized it with a citrate ligand for an enhanced redox property and better solubility in water. For structural analysis of the nanohybrid, standard analytical tools, such as electron microscopy, dynamic light scattering, and X-ray diffraction studies were conducted. Moreover, FTIR and UV-VIS spectroscopy studies were performed to confirm its functionalization. The antibacterial study results, against a model bacteria (*S. hominis*), show that CuO nanohybrids provide favorable outcomes on antibiotic-resistant organisms. The suitability of the nanohybrid for use in photodynamic therapy was also confirmed, as under light its activity increased substantially. The use of CuO nanoparticles as antibiotics was further supported by the use of computational biology, which reconfirmed the outcome of our experimental studies. We have also extracted CuO nanogranules (top-down technique) from copper mine tailings of two places, each with different geographical locations, and functionalized them with citrate ligands in order to characterize similar structural and functional properties obtained from synthesized CuO nanoparticles, using the bottom-up technique. We have observed that the extracted functionalized CuO from copper tailings offers similar properties compared to those of the synthesized CuO, which provides an avenue for the circular economy for the utilization of copper waste into nanomedicine, which is known to be best for mankind.

Keywords: copper nanohybrid; citrate functionalized CuO; nano-medicine; *S. hominis* infection control; photodynamic therapy

1. Introduction

Copper was the first metal discovered in the history of human civilization during the chalcolithic or copper age, around 6000 years ago. This marvel metal was well known in ancient times, not only for its ability to enhance the strength of the tools, but also for its impressive healing capacity. The ancient Indians, Greeks, and Egyptians all used copper containers for water purification, treatment of wounds, and lung ailments. Copper cooking

utensils were employed throughout the Roman empire to stop the spread of disease [1]. In recent times, the US Environmental Protection Agency (EPA) has classified copper and its derivatives as antibacterial materials [2]. On the other hand, the presence of copper in the human body is essential for healthy development, cardiovascular and lung functionality, neovascularization, neuroendocrine function, and iron metabolism [3].

Metallic copper, cupric oxide (CuO), and cuprous oxide (Cu_2O) nanoparticles are attracting considerable research interest nowadays due to their widespread applications in catalysts and therapeutic domains [4–10] compared to their bulk counterparts, by virtue of their nano dimensional higher surface area to volume ratio. Specifically, copper oxide nanoparticles (CuO NPs) display broad-spectrum antibacterial and photocatalytic properties [11] and have the potential to be used as an alternative to antibiotics. The design and development of new compounds as antibiotics possess an emergent need, as the overuse and misuse of existing antibiotics are responsible for the growing episodes of antibiotic-resistant infections and deaths globally [12].

The antibacterial activity of CuO NPs against Gram-positive bacteria, such as *S. aureus* and *B. subtilis* as well as Gram-negative bacteria, such as *E. coli* and *P. aeruginosa* are reported in various studies [13–17]. Metallic Cu and CuO NPs are also found to exhibit multi-toxicity on multi-drug resistant bacterial species, such as the methicillin-resistant S. aureus (MRSA) [18]. In the case of CuO NPs, it is suggested that its antibacterial effect might be associated with cell membrane dissociation and reactive oxygen species (ROS) production [19]. Various simultaneous mechanisms of action of CuO nanoparticles against bacteria make it almost impossible for the microbes to develop resistance, as the bacterial cell would be required to generate multiple simultaneous gene mutations to develop this resistance [20]. Copper oxide nanoparticles are obtaining growing attention for their cheaper price and abundance in comparison with other noble and expensive metals, such as silver and gold, and their competent potential application as microbial agents [15,21,22].

The size, morphology, and solubility play a significant role in the antibacterial activities of Cu, CuO, and Cu_2O [23–25]. However, the major limitation of metallic CuO NPs in the nano-size range is the lack of significant stability in dispersions, due to their strong tendencies to aggregate and the formation of larger clusters that reduce the energy associated with their high surface area [26–28]. The formation of clusters results in sedimentation leading to loss of reactivity and antimicrobial performance, in which a nanometric size is essential [28]. Further surface modifications of CuO NPs using a post functionalization approach, not only enhances their colloidal stability, yet can also introduce unique physical and chemical properties, including the possible enhancement of their antimicrobial activities. Functionalization, or capping of an inorganic nanoparticle with an organic ligand-like citrate or folate, is evidenced to produce nanohybrids that have unique therapeutic potentials [29].

In the current study, we have explored the effect of citrate-capped CuO NPs on a Gram-positive *Staphylococcus hominis* (SH) bacterial strain. Indeed, *S. hominis* is a commensal bacteria that resides on human skin [30]. Although it is apparently harmless, it has been reported that one of its subspecies, novobiosepticus, is multidrug-resistant and causes nosocomial infections, such as sepsis, alongside bloodstream infections in neonates and immunocompromised patients [31], and various opportunistic infections of humans [32]. *S. hominis* is also well known for its ability to generate pungent body odor in humans [33]. In the present study, we have reported the synthesis or extraction, characterization, and antimicrobial activity of citrate functionalized CuO NPs on the Staphylococcus hominis bacterial strain. CuO NPs were synthesized and capped using a precipitation technique [34] and grafting method [35], respectively, in a bottom-up approach. Similarly in a top-down method, CuO NPs were extracted, and citrate functionalized from two types of copper-containing stones from copper mines. The structural properties of both synthesized and extracted CuO NPs were examined by X-ray diffraction (XRD), and field emission scanning electron microscopy (FESEM), which were equipped with an energy dispersive X-ray spectroscopy (EDS) and found to be similar. Dynamic light scattering (DLS) and zeta potential studies were also employed for estimating the hydrodynamic diameter

and solubility assessment of the synthesized nanohybrid. The surface functionalization of CuO NPs by citrate ligands was confirmed by FTIR and UV-vis spectroscopy. The antimicrobial activity of citrate-CuO NPs was examined in the *S. hominis* bacteria strain. The citrate functionalized NPs were found to generate reactive oxygen species (ROS) upon photoexcitation, which is responsible for their antimicrobial action because ROS has the ability to destroy the active substances in the bacterial inner and outer membranes [36–38]. This phenomenon establishes the credentials of citrate CuO NPs for applications including antibacterial photodynamic therapy (PDT) with enhanced efficacy. We have also used computational biology strategy in order to rationalize the antibiotic-resistant bacterial remediation found in our experimental studies.

Immediately after the establishment of the CuO nanohybrid as a potential antibacterial agent, we also explored the use of copper mine tailings as a source of raw materials used for the nanohybrid synthesis, in order to simultaneously cater to low-cost antibiotics to a wider population across the globe and to remediate the burden from the copper mines. We have also developed a prototype FMCG product (talcum powder) for the remediation of bacteria *S. hominis* which are responsible for the generation of several human disorders.

2. Materials and Methods

2.1. Materials

Copper acetate, citric acid, sodium hydroxide, and sodium citrate were purchased from Sigma Aldrich (St. Louis, MO, USA), California. All solvents and all other used chemicals were procured from Merck (New Jersey, USA), unless otherwise stated. 2,7-dichlorodihydrofluorescein diacetate (DCFH-DA) was bought from Calbiochem to estimate the reactive oxygen species (ROS) production. Similarly, 2,2-diphenyl-1-picrylhydrazyl (DPPH) was obtained from Sigma (St. Louis, MO, USA) to monitor the antioxidant activity in the samples. All reagents were analytical grade and used without any further purification. Nanopore water, with a resistivity value $\geq 18\,M\Omega$ cm, from the Milli-Q system (Millipore GmbH, Germany) was used in all experiments. For bacterial studies, LB top agar and Luria broth (LB) medium were purchased from HIMEDIA. The Gram-positive bacteria, Staphylococcus hominis (*S. hominis*) strain, was procured from ATCC.

2.2. Synthesis of Functionalized CuO Nanoparticles

In this study, the CuO NPs were synthesized following the reported precipitation method by Zhu et al. [34]. The citrate ligands generated in the process provided satisfactory passivation against aggregation and sufficient stability to the NPs in colloidal suspension. Briefly, 150 mL of deionized water was used to dissolve 0.54 g of copper acetate. Next, 0.52 g of citric acid was added, and the mixture was vigorously stirred while being heated to boiling at 100 °C. Once the mixture's pH attained a value of 6–7, 0.7 gm or 0.015 mol of sodium hydroxide (NaOH) was added quickly, causing a significant amount of dark brown precipitate to form at the same time. The blue color solution was immediately converted to brown, indicating the production of CuO NPs. The liquid was cooled to room temperature while being stirred after 5 additional minutes of reflux. The CuO-NPs were subsequently separated by centrifugation (4000 rpm, 10 min), and washed twice with water and another two times with ethanol. The supernatant, which contains citrate-capped CuO NPs, was then separated.

Using the citric acid grafting procedure, the CuO NPs were further functionalized. In a water-to-ethanol ratio of 8:2, suspensions of 200 mM acetic acid and 65 mM CuO were performed. The produced citric acid solution was combined with the CuO suspension, and the pH of the resulting combination was raised to 12 by adding 6 M NaOH. Next, the mixture was refluxed for three hours. The product was then centrifuged and properly cleaned three times to remove the extra citric acid. To obtain citrate-capped CuO (C-CuO) from the two copper tailings in the mines of Peru and Bhopal (India), a similar procedure was followed. Only 160 mg of each stone dust was mixed initially with 150 mL of deionized water before the addition of citric acid and boiling occurred.

2.3. Characterization Tools and Techniques

Optical absorbance spectra of samples were measured in a double-beam UV-vis spectrophotometer (model UV-2600, Shimadzu, Japan) in the 200−800 nm wavelength range. The room temperature steady-state emission spectra were recorded using a Fluorolog Model LFI-3751 (Horiba-Jobin Yvon, Edison, NJ, USA) spectrofluorometer equipped with a microchannel plate−photomultiplier tube (MCP−PMT, Hamamatsu, Japan). All fluorescence spectra were corrected for variations with a wavelength in source intensity, photomultiplier response, and monochromator throughput. The X-ray diffraction (XRD) pattern of synthesized CuO nanoparticles was measured in a PANalytical X'PertPRO (Malvern Panalytical Ltd., Malvern, UK) diffractometer, with Cu Kα radiation (at 40 mA and 40 kV) generating at a rate of 0.02 $^\circ$ s^{-1} in the 2θ range from 20 $^\circ$ to 80 $^\circ$. The liquid CuO nanoparticles were subjected to lyophilization for the XRD analysis. We have performed Fourier transform infrared spectroscopy (FTIR) on the liquid samples and the spectra were obtained using a JASCO FTIR-6300 spectrometer instrument (Oklahoma city, OK, USA). A NanoS Malvern (Zeta-seizer) instrument equipped with a 4 mW He:Ne laser (λ = 632.8 nm) and a thermostat coupled sample chamber was employed for dynamic light scattering (DLS) and ζ potential measurements. Quartz cuvettes of 10 mm path length were used to execute all spectroscopic experiments. The structural morphologies and chemical compositions of the synthesized citrate CuO nanohybrids from different sources were analyzed using scanning electron microscopy (SEM) and EDAX methods. Before scanning in a field emission scanning electron microscope (Quanta FEG 250: source of electrons, FEG source; operational accelerating voltage, 200 V to 30 kV; resolution, 30 kV under low vacuum conditions: 3.0 nm; detectors, large field secondary electron detector for the low vacuum operation), the coverslips containing samples were coated with gold.

2.4. Antioxidant Activity

The free radical scavenging capability of the samples of interest was determined using the DPPH assay method. A 0.15 mM DPPH solution was prepared in methanol and 0.5 mL citrate CuO nanoparticles of various concentrations were added to 2.5 mL of the freshly prepared DPPH solution. The characteristic absorption maxima of DPPH at 535 nm were selected to monitor the degradation process with DPPH in the presence and absence of light at room temperature. The absorption spectra of DPPH were recorded in the interval of 2 s for an hour using SPECTRA SUITE software provided by Ocean Optics.

2.5. Quantification and Characterization of ROS

For the purpose of quantifying the generated ROS, we used 2′,7′-dichlorofluorescein (DCFH), which is a well-known reagent. The DCFH was prepared via a de-esterification reaction from DCFH-DA at room temperature, following a standardized protocol described in previous studies [39,40]. The oxidation of DCFH, in the presence of light, leads to the production of DCF emitting fluorescence [41,42]. In this study, the ROS generated in the aqueous citrate functionalized CuO NPs convert DCFH into DCF, which has a characteristic emission maximum of 522 nm upon excitation at 488 nm. The DCF emissions were recorded in the Fluorolog Model LFI-3751 (Horiba-Jobin Yvon, Edison, NJ) spectrofluorometer. The ROS experiments were performed in the dark and in the light for 30 min.

2.6. Bacterial Strain and Culture Conditions

The antibacterial activity of the synthesized and extracted samples have been investigated against a strain of Staphylococcus hominis bacteria. The Gram-positive *S. hominis* strain was procured from ATCC. For the antibacterial assay, fresh *S. hominis* bacteria have been cultured using sterilized Luria–Bertani (LB) medium in a shaker incubator at a temperature of 37 $^\circ$C for 24 h. All used glassware, suction nozzle, and culture medium were sterilized in an autoclave at a high pressure of 0.1 MPa and a temperature of 120 $^\circ$C for 30 min prior to the experiments beginning. The treatment of bacteria was performed on LB agar plates using the colony forming unit (CFU) assay method under dark and light

illumination conditions. The freshly grown original *S. hominis* bacterial suspension was firstly washed twice with phosphate-buffered saline (PBS; pH 7.4) solution and further diluted 10^6 times before the test samples were added. Then, they were incubated with the respective nanoparticles for 1 h. The resulting bacterial PBS suspensions (200 µL) were uniformly spread over gelatinous LB agar plates and cultured at 37 °C for 24 h to obtain the CFUs. To quantify the antibacterial activity, the number of survival colonies was manually counted and presented as a bar diagram.

Detection of microbial growth was also performed in the cuvette system for different citrate CuO NPs under various conditions. For this bacterial mortality study, a bacterial solution of 10^8 CFU/mL was considered and incubated with test solutions of 1 mM concentrations, initially for 3 h with photoactivation.

For the cuvette-based detection of microbial growth, the cells were cultured in an LB medium under an incubator shaker at 37 °C for 24 h. The optical density of the freshly grown overnight culture was fixed to 0.1 in LB medium initially. The culture was then put into a cuvette, mixed with the test samples, and incubated at 37 °C for 9 h with shaking under dark and illumination conditions. The absorbance was taken at 1 h intervals and plotted against time, with baseline correction for studying the growth curves.

For the microscopic studies, the bacteria cells after proper incubations with the nanoparticles were stained with DAPI and PI. DAPI stains all cells, while PI only stains the membrane-disrupted cells. The (1-red/blue) ratio was obtained to assess the viability of the *S. hominis*. The tests were repeated three times. The samples (15 µL) were observed under a fluorescence microscope (Leica digital inverted microscopes DMI8).

2.7. Statistical Analysis

All the data in this current work are represented as mean ± standard deviation (SD), unless otherwise stated. An unpaired 2-tailed *t*-test was used for comparison between the groups. A value of $p < 0.05$ was considered significant. GraphPad Prism (v8.0) software was used for all statistical tests.

2.8. Method of Computational Biology

The web resource STITCH (http://stitch.embl.de/; accessed on 24 December, 2022) was utilized to predict the chemical–protein (CP) interaction networks of CuO NP in *S. hominis*. The STITCH database can forecast around 960,000 proteins and 430,000 compounds from the 2031 eukaryotic and prokaryotic genomes [43,44]. The confidence score of a chemical–protein interaction can be used to predict the relationship, with a higher value indicating a stronger interaction. For the purposes of this investigation, a medium confidence score of 0.4 was taken into account.

3. Results and Discussion

X-ray diffraction (XRD) characterization of the synthesized and extracted CuO NPs was carried out to estimate the precise elemental composition, particle size, and superficial morphology, as depicted in Figure 1a. It was determined that all CuO NPs were in a monoclinic geometry with a space group of C2/C. No characteristic peaks of any other impurities were detected, suggesting the preparation of high-quality CuO NPs. Moreover, the obtained χ^2 value of 1.82 for the Le Bail fitting indicates excellent agreement with the previously reported literature [45,46]. The crystallite size is estimated from the XRD pattern using Debye Scherrer's Equation (1) [47]:

$$D = K\lambda / \beta \cos \theta \qquad (1)$$

where $K = 0.94$ is the shape factor, λ is the X-ray wavelength of Cu Kα radiation (1.541 Å), θ is the Bragg diffraction angle, and β is the full width at half maxima (FWHM) of the respective diffraction peak. The crystallite size corresponding to the highest peak observed in XRD was found to be 34.4 nm. The presence of sharp structural peaks in XRD patterns and a crystallite size less than 100 nm corresponds to the nanocrystalline nature of

synthesized CuO NPs. The peaks at 32.5, 35.4, 35.5, 38.7, 38.9, 46.2, 48.8, 51.3, 53.4, and 56.7 in 2θ correspond to the different CuO planes [48]. Similarly, as shown in Figure 1a, the CuO obtained from Peru and Bhopal mine samples exhibited peaks corresponding to the synthesized CuO NPs. The peaks at the same 2θ positions for the extracted CuO nanoparticles from both Peru and Bhopal mine samples are referred to here and confirm the extraction of CuO from the mine samples. The additional peaks appear due to the attribution of elements such as Au, Cr, etc., which are present in the mine samples, as revealed from the SEM EDAX analysis (Figure 2).
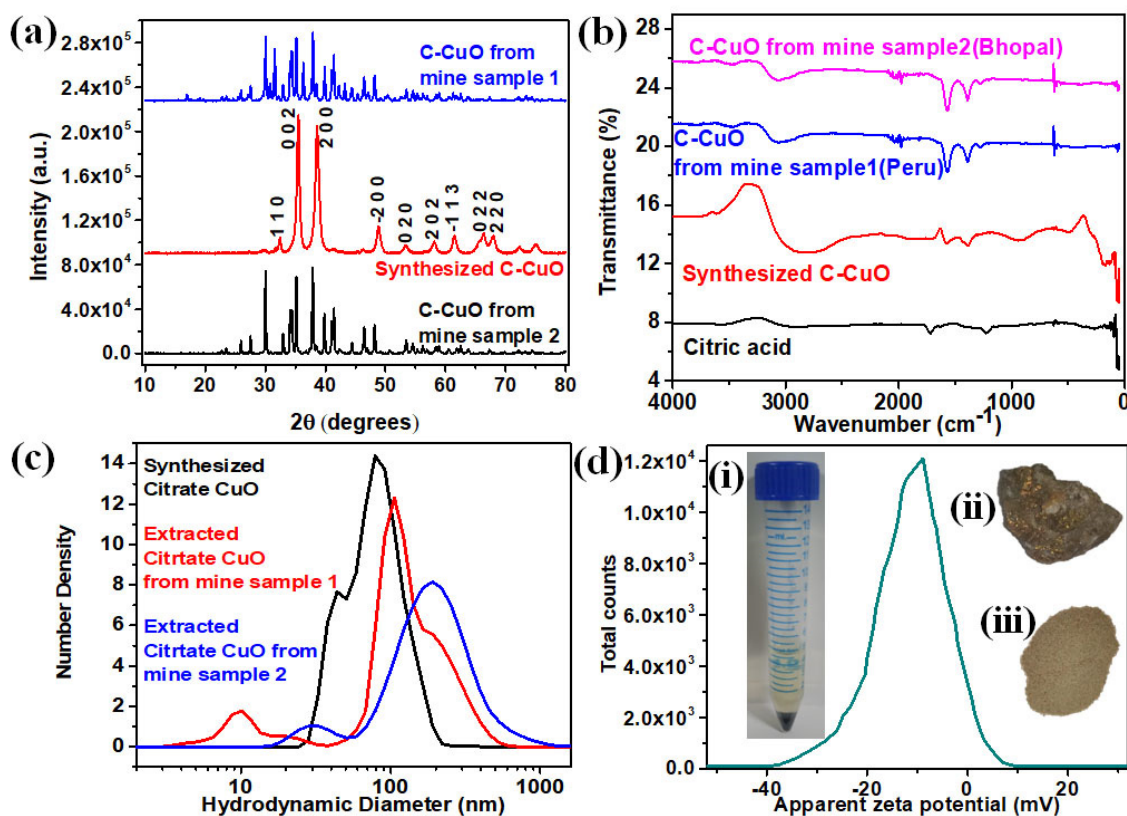
Figure 1. (**a**) XRD of the synthesized and extracted (from Peru and Bhopal samples) CuO nanoparticles. (**b**) FTIR spectra of different citrate-capped CuO samples and citric acid in the range between 0 and 4000 cm^{-1}, (**c**) DLS of the citrate-capped CuO from supernatants of C-CuO samples, (**d**) zeta potential distribution of the synthesized citrate functionalized CuO NP. The insets (i), (ii), and (iii) of Figure 1d are the synthesized C-CuO, the Peru mine tailing, and the Bhopal mine sludge, respectively.

To ensure the surface functionalization of the synthesized and extracted CuO NPs by citrate, FTIR analysis was performed on citric acid and the nanoparticles (Figure 1b). The absorption band, around 620.9 cm^{-1} in synthesized citrate CuO (C-CuO), C-CuO from mine sample 1 (Peru), and C-CuO from mine sample 2 (Bhopal) can be attributed to the vibrations of the Cu−O group [49,50]. Furthermore, the absence of other molecular vibrations, due to the calcination of the synthesized C-CuO, confirms the formation of a pristine surface. The citric acid was found to exhibit an absorption band occurring at around 1718 cm^{-1}, which is attributed to the C=O stretching, while the band occurring at 1394 cm^{-1} is attributed to the C−O stretching [51]. Moreover, the signature of the O−H stretching from the tertiary alcohol of citric acid can be witnessed at around 1099 cm^{-1}, and the bending of the O−H group from the carboxylic acid portion can be observed at 1383 cm^{-1}. Finally, the absorption band at 3299 cm^{-1} is due to the presence of the O−H bond from the citric acid. In the CuO FTIR spectrum, the C−O and C=O stretching can be seen at 1370 cm^{-1} and around 1600 cm^{-1}, while the tertiary alcohol band is at 1080 cm^{-1}. The shift in C=O and

C−O indicates that the CA is bonded to the CuO via the chemisorption of the carboxylate group. Therefore, the weakening of C=O causes a shift in frequency from 1700 to 1600 cm^{-1}. This characterization confirmed the success of the surface modification of CuO with citric acid. All the FTIR spectra shown in Figure 1b are baseline corrected; however, the apparent baseline shift may be due to the excess concentration of the synthesized citrate CuO nanoparticles in comparison with the extracted CuO NPs from the copper mine tailings.
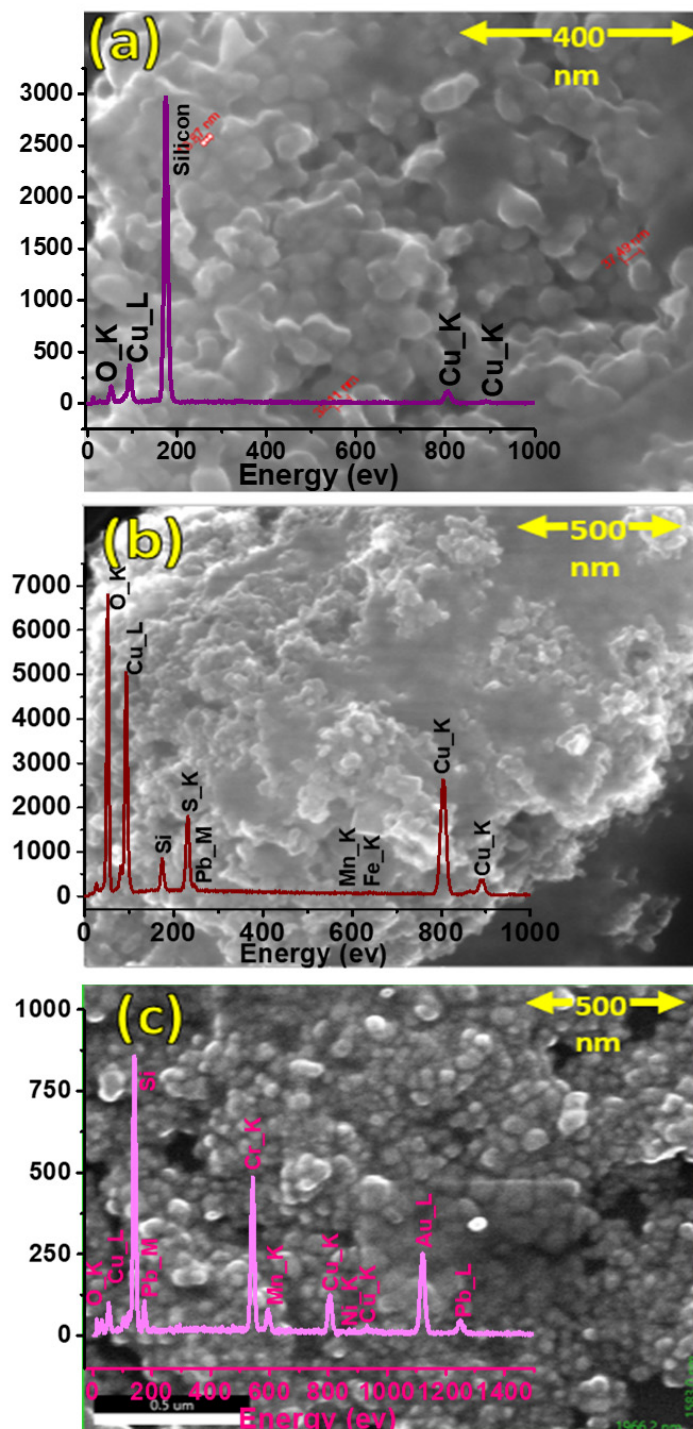
Figure 2. FESEM images of (**a**) synthesized citrate-capped CuO NPs. The inset shows the EDAX parameters of the nanoparticles. (**b**) Extracted and citrate-capped CuO from Peru mine stone sample. The inset shows the EDAX parameters of the nanoparticles. (**c**) Extracted and citrate-capped CuO from the Bhopal mine stone sample. The inset shows the EDAX parameters of the nanoparticles.

The hydrodynamic diameter of the synthesized CuO nanohybrid, C-CuO mine sample 1 (Peru) and 2 (Bhopal) were estimated to be 78.8 nm,106 nm and190 nm, respectively, from the dynamic light scattering (DLS) studies (Figure 1c), which are close enough to each other. The results of the DLS corroborate with the size obtained from the XRD (34.4 nm) and FESEM analyses (38.1 nm). Dynamic light scattering (DLS) accounts for the hydrodynamic diameter of the functionalized nanomaterial, which comprises core CuO and citrate ligands at the surface, along with associated water molecules and some possible aggregation of the functionalized nanoparticles in the aqueous solution. The electron micrograph of the nanoparticles shows the inorganic nanomaterial, as a whole, contains crystalline and amorphous inorganic core substrate. On the other hand, the size from the XRD accounts for only the crystalline materials in the core inorganic particles. Thus, it is obvious that DLS overestimates the size, while XRD reveals the crystalline nanoparticles in the core [52]. Additionally, the citrate CuO NPs exhibited a ζ-potential of magnitude -10.38 mV, assuring moderate solubility of the NPs (Figure 1d). The ζ-potential for the Peru and Bhopal samples were obtained to be -11.2 mV and -8 mV, respectively. These results lower the possibility of instability and particle agglomeration or precipitate tendencies of the CuO NPs out of the solutions. The full curve for a sample is only provided by the instrument software, while the titration experiment was performed because we obtained a synthesized pure citrate-capped CuO nanohybrid. However, for the extracted citrate CuO nanoparticles from Peru and Bhopal mine samples, only zeta potential measurements were carried out, for which only values in the mV unit are provided because, as mentioned previously, no full curves were available from the instrument. The insets in i, ii, and iii of Figure 1d are the synthesized C-CuO, the Peru mine tailing, and the Bhopal mine sludge, respectively.

Figure 2a–c shows the FESEM images of the C-CuO NPs. The inset of Figure 2a depicts the EDAX spectrum of the synthesized CuO NPs. The EDAX analysis of the extracted citrate CuO from the Peru and Bhopal mine tailings are shown in the insets of Figure 2b,c. The EDAX result shows that there are no other elemental impurities present in the prepared CuO NPs. However, trace amounts of Au and Cr, etc., were found in the extracted CuO NPs from the EDAX method. The peak of silicon appearing in the EDAX graphs of Figure 2 is attributed to the substrate. For EDAX analysis, the test sample was a drop cast on a Si wafer substrate and the thickness of the drop casted layer may not be uniform throughout the substrate. In the FESEM images of C-CuO, the synthesized nanohybrids are seen to consist of clustered spherical particulates with approximate diameters between 38 and 46 nm. The average diameter of the CuO NPs was calculated by measuring over 100 particles in a random field of FESEM view. The SEM-EDAX analysis demonstrated that the atomic compositions of the Cu and O elements were 38.41% and 61.59%, respectively. The mean ratio of Cu and O was, therefore, 38.41:61.5, and an accurate compound formula based on this atomic ratio of Cu and O can, thus, be given as $Cu_{1.2}O$ or $CuO_{0.8}$. Therefore, it can be ensured that most of the synthesized nanoparticulate sample was indeed CuO.

The UV-vis spectra of the citrate-capped CuO samples (Figure 3a) exhibited a broad absorbance peak at 285 nm, which is characteristic of a surface plasmon resonance of the CuO nanoparticles [53]. A weaker peak at around 350 nm, signifies the d–d transition of CuO nanoparticles due to citrate functionalization and the quantum confinement effect of the CuO NPs on the citrate functionalization [54]. Similarly, the peaks observed at 285 nm and 350 nm, after the capping of Peru and the Bhopal samples, signified the presence of citrate-capped CuO NPs within the system.

The dark and photoinduced ROS generation capability of the citrate CuO NPs is illustrated using a well-known nonfluorescent probe: DCFH (Figure 3b). DCFH is oxidized to fluorescent dichlorofluorescein (DCF) by ROS, exhibiting an emission near 522 nm upon excitation at 488 nm. Thus, the enhancement of the ROS generation level is indicated by the increase in the emission intensity at 522 nm [37]. The oxidation of only DCFH control and CuO NPs are monitored for 35 min in the dark and then under irradiation of UV light (365 nm). In the dark, there is a considerable enhancement of emission intensity at 522 nm, indicating the presence of dark ROS generation. However, with light exposure, a greater

increase in emission intensity is observed for the citrate CuO nanohybrid compared to the control (Figure 3b). This confirms the ROS generation capability of the synthesized nanohybrid under light exposure making it suitable to apply for photodynamic therapy.
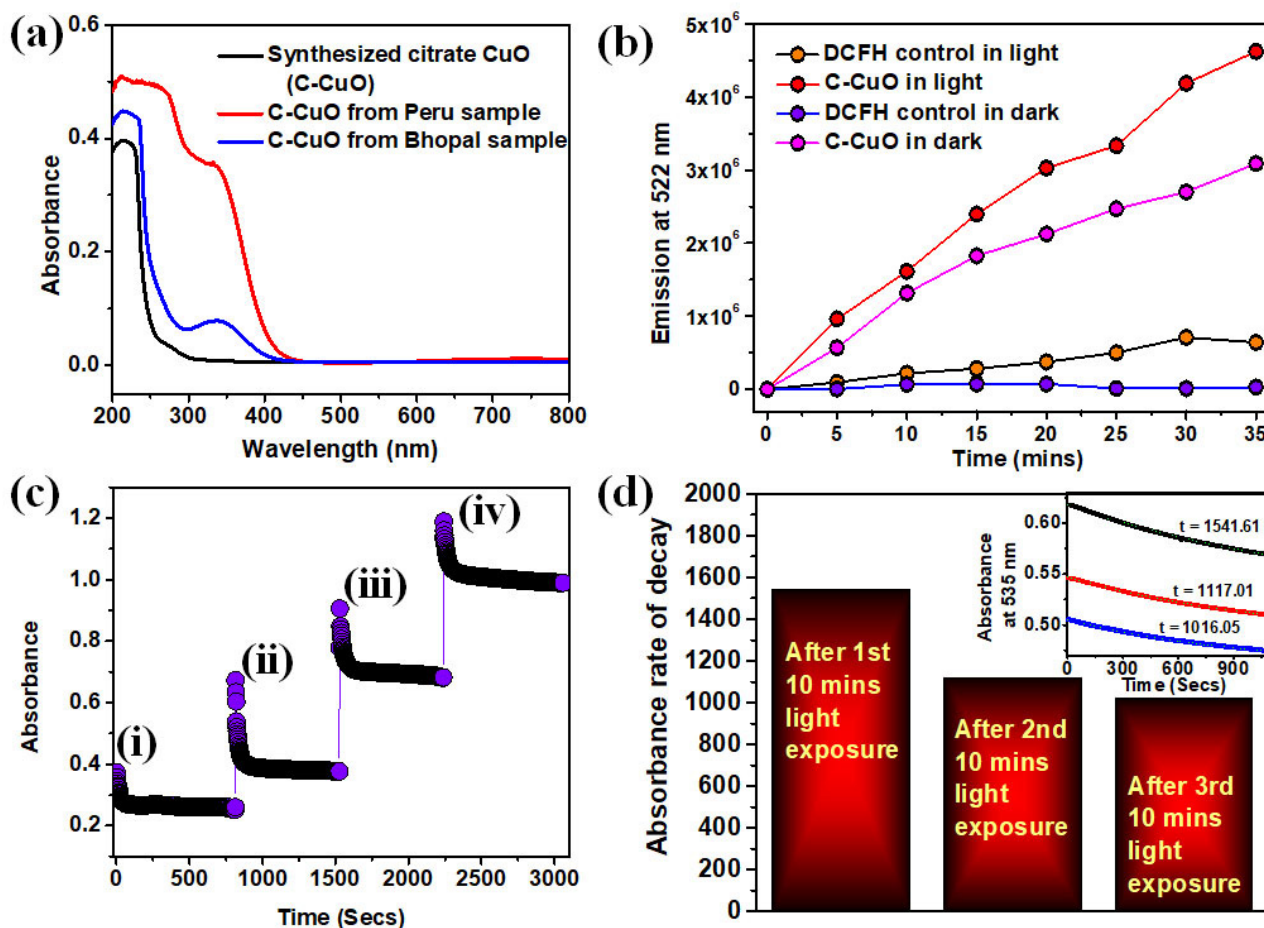

Figure 3. (**a**) Absorbance spectra of synthesized and extracted citrate-CuO nanohybrids. (**b**) DCFH oxidation (monitored at 522 nm) with time in the presence and absence of citrate CuO NPs under dark and illumination conditions. (**c**) The DPPH catalytic activity of the synthesized CuO NPs in dark conditions upon the addition of DPPH in periodic intervals of time (i) (ii) (iii) and (iv). (**d**) The DPPH assay of the synthesized CuO NPs under UV light illumination conditions. Inset shows the decay of absorbance of DPPH radical at 535 nm with multiple light exposures of 10 min intervals.

The antioxidant activity of the citrate functionalized CuO NPs was evaluated using the DPPH assay method (Figure 3c,d). The absorbance of DPPH at 535 nm was observed to decrease with time, establishing the presence of antioxidant properties of the CuO NPs under dark conditions and with a visual transition of the solution from purple to yellow. Now, upon further addition of 50 uM DPPH, after a periodic interval of time, it is observed that the free radical scavenging activity remains almost intact in the same 100 uM C-CuO sample. The study of antioxidant activity in the presence of UV light (365 nm) is a prerequisite to a full understanding of its potential antioxidant properties. As shown in Figure 3d, the rate of absorbance at 535 nm decreases (from 1541.51sec to 1117.01sec to 1016.05sec) with UV exposure of 10 mins for each case, keeping the concentrations of DPPH and C-CuO NPs to be constant. The results corroborate the enhancement of antioxidant activities with light exposure. The same sample of C-CuO NPs is capable of providing catalytic activities after getting recharged by light exposure.

The antibacterial activities of the C-CuO NPs, synthesized and extracted from nine samples were investigated against Gram-positive *S. hominis* bacteria by analyzing their

growth curves. Figure 4a reveals the growth pattern of the bacteria in terms of absorbance at 600 nm with one-hour intervals. The synthesized C-CuO, under illumination as well as dark conditions, is observed to almost nullify the growth, with respect to the controls where only the bacteria are present in LB media. The C-CuO extracted from the Peru and Bhopal mine samples are observed to exhibit better antimicrobial activity in presence of light. The copper chloride salt used for the synthesis of CuO NPs, and sodium citrate used for the capping purpose were found to have almost no effect on bacterial growth, establishing the fact that the entire antimicrobial activities are solely generated by the C-CuO NPs.
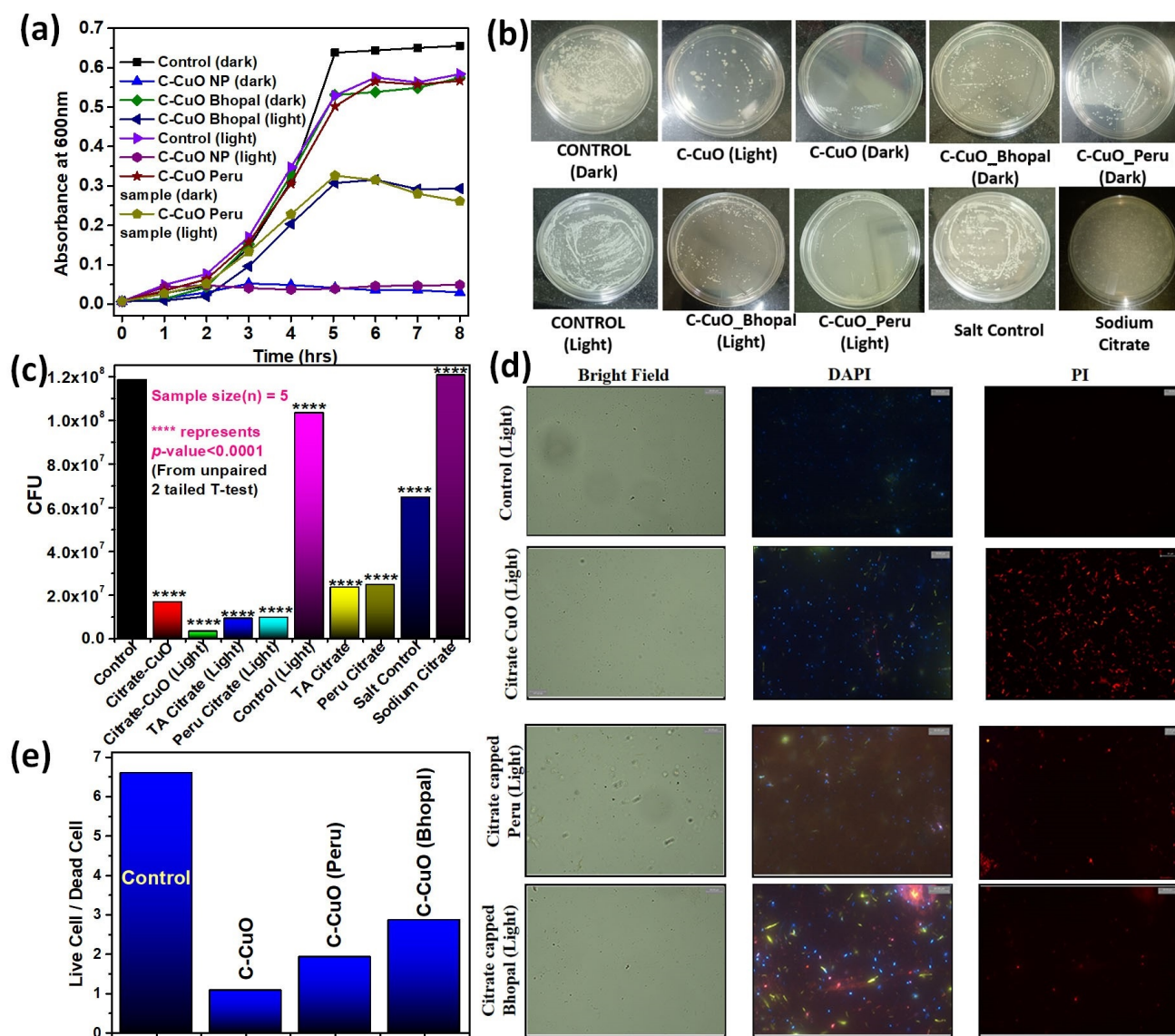

Figure 4. (**a**) Effect of C-CuO NPs on the growth curves of *S. hominis* bacteria under dark and illumination conditions. (**b**) Bacterial viability after treatment with different citrate CuO NPs in the presence and absence of light irradiation. (**c**) Agar plate colony count assay. '****' indicates *p*-value < 0.0001. (**d**) Bright-field microscopic images and fluorescence micrographs of bacteria stained with DAPI, and fluorescence micrographs of bacteria stained with PI. (**e**) The ratio of live and dead cells obtained from microscopy.
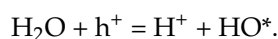
The antimicrobial activity of the synthesized and extracted CuO NPs after citrate functionalization was investigated against *S. hominis* growth to explore the antibiotic potential against bacterial infections in the agar plate assay method. To probe the antibacterial action of the nanoparticles, they were used for incubating the culture for 3 h. As shown

in Figure 4b,c, minimal colonies were observed (the bacterial growth was found to have decreased by 96.9% in the CFU from the control plate) for the nanohybrid under UV light illumination conditions. The bacterial growth is found to be decreased by 85% only in the CFU under dark conditions. The effect of two different mine-extracted copper nanohybrids under dark and light irradiation conditions was then studied further upon the growth of *S. hominis* bacteria (Figure 4b). In the case of the Peru and Bhopal samples, the bacterial growth is found to be decreased by 79% CFU and 80% CFU, respectively, in dark conditions. On the other hand, a huge decrement in bacterial growth is observed for both the Peru and Bhopal samples after citrate-capping on UV illumination. The bacterial growth was reduced by 90% and 91% for the citrate-capped Peru and Bhopal samples, respectively, on the UV illumination. To nullify the effect of the salt and the capping agent (sodium citrate), their antibacterial effects were studied. No significant change in the number of colonies in the negative control group was found, indicating a low antibacterial effect of these salts on *S. hominis*. Thus, the antibacterial effect found is solely due to the citrate-capped CuO NP. From these results, it is evident that the nanohybrid is itself an antibacterial agent and its efficiency enhances many folds upon white light exposure, which triggers an overall huge antibacterial effect.

To study the effect of the citrate CuO nanohybrid, bacterial cultures were performed five times for each group (control in dark and light, citrate CuO in dark and light, different concentrations of the nanohybrid, etc.) and their differences were calculated to identify their significance levels. The sample size for each of the groups was five. The *p*-value was calculated using an unpaired 2-tailed *t*-test and a value of $p < 0.05$ was considered to be significant. The statistical difference between the control and treatment is designated by '*'. The '*' represents a *p*-value < 0.1 and '****' represents a *p*-value < 0.0001 [55].

The antimicrobial activity of the NPs was further investigated using optical microscopy. We used *S. hominis*, the Gram-positive bacteria, as the model biological system. *S. hominis* were incubated with both synthesized and extracted CuO samples for two hours in LB broth and then stained with DAPI and PI. While DAPI stains all the cells in the medium, PI is specific to dead cells as it cannot cross intact cell membranes. Therefore, the ratio of DAPI-stained cells to PI-stained cells reveals the viability of the cells. Figure 4d,e shows the results of the microscopic microbial studies. The first row of Figure 4d contains the microscopic images of the control cells after staining with DAPI and PI. As expected, the number of viable cells was more than the dead cells (ratio ~6.6). The microscopic images of the synthesized C-CuO NPs (Figure 4d, second row) incubated with bacteria showed a reduced ratio–i.e., the dead cells outnumbered the live cells (ratio ~2.1) compared to the control. Interestingly, the group of bacteria treated with C-CuO NPs extracted from the Bhopal and Peru mine samples (Figure 4d, rows 3 and 4) also showed higher viability compared to the control. The ratio for these C-CuO NP-treated groups was similar to that of the synthesized C-CuO-treated group, as shown in Figure 4e. Therefore, the microscopic studies revealed that the C-CuO NPs exerted toxic effects and effectively killed the *S. hominis*. The therapeutic action of the CuO NPs against *S. hominis* bacteria occurs primarily via the generation of reactive oxygen species, which mainly includes the formation of hydroxyl radicals (HO.*) and superoxide radicals (O_2^{-*}). Initially, electron-hole (e⁻/h⁺) pairs are formed when the electromagnetic radiation of energy (hυ) is either greater than or equal to the bandgap energy (E_g) of the CuO NPs. This phenomenon excites the electron from the valence band (VB) to the conduction band (CB), leaving holes behind in the VB. These photoexcited electrons reduce the surface adsorbed O_2 to O_2^-., while the holes oxidize H_2O or HO- to OH* [56–58], as described in the graphical abstract. This in situ production of the reactive radicals starts off by attacking the bacterial population and eliminates them through the production of toxic by-products, resulting from ROS-mediated damage to the cellular system.

$$CuO + h\upsilon = CuO\ (e^- + h^+)$$

$$O_2 + e^- = O_2^{-*}.$$

$$H_2O + h^+ = H^+ + HO^*.$$
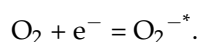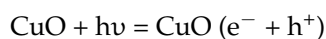
In the absence of electromagnetic radiation, the antimicrobial activity may be attributed to the ligand-to-metal charge transfer (LMCT) of the C-CuO NPs. The LMCT bands originate due to the interaction of the $Cu^{1+}/^{2+}$ centers in the NP with the surface-bound citrate ligands. In the dark condition, the origin of the antibacterial activity might be due to the conversion of the Cu^{1+} to Cu^{2+} states at the center, accompanied by the direct injection of the electrons into the CB of the C-CuO NPs and followed by the reduction of the surface adsorbed O_2 to O_2^-.

$$Cu^{1+} - O = Cu^{+2} - O^* + e^-$$

$$O_2 + e^- = O_2^-$$
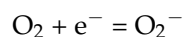
The enhanced efficacy of the citrate functionalized CuO NPs, in the presence of light for more bacterial remediation, establishes its credentials for the application of APDT (antibacterial photodynamic therapy).

The extraordinary effect of the synthesized copper nanohybrid may be hypothesized using predictive biological interactions. To compare our findings with the existing research and related predictive models, the previously mentioned STITCH database was used. It generated an interaction network (Figure 5) between the ligand CuO and its effect on various proteins of *S. hominis*. To understand how CuO affects the survival of the bacteria, a comprehensive table (Table 1) was populated with the protein names and their respective activities. The table suggests the negative impact of CuO on key proteins of *S. hominis*, which helps the organism deal with environmental stress, energy metabolism, GTP binding, and translation regulation, etc.
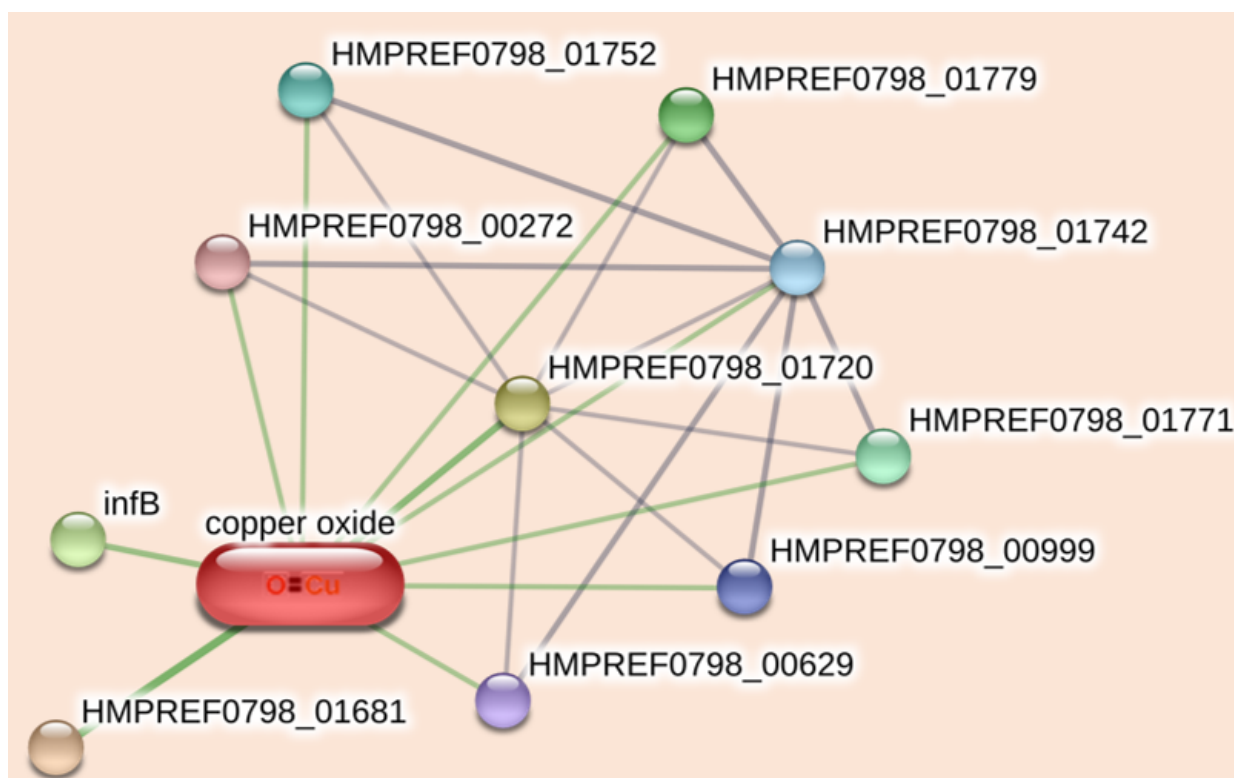
Figure 5. Compound protein interactions network of citrate CuO nanohybrid on *S. hominis* bacterial strain.

Table 1. Effect of citrate functionalized CuO NPs on *S. hominis* bacterial strain.

Identifier	Corresponding Protein Name	Activity
HMPREF0798_01720	Catalase	Catalase, an antioxidant enzyme found in all aerobic organisms, facilitates the transformation of H_2O_2 into water and oxygen under environmental stress. [59]
HMPREF0798_01742	Pyridine nucleotide-disulfide oxidoreductase family protein	Controls mitochondrial function. [60]
HMPREF0798_00999	Pyridine nucleotide-disulfide oxidoreductase	
HMPREF0798_01779	Dihydrolipoyl dehydrogenase	This oxidoreductase is a key factor in bacterial pathogenesis and is responsible for energy metabolism [61]
HMPREF0798_01752	Dihydrolipoyl dehydrogenase	
HMPREF0798_00272	Dihydrolipoyl dehydrogenase	
HMPREF0798_00629	Dihydrolipoyl dehydrogenase	
HMPREF0798_00484, infB	Translation initiation factor, IF-2	IF2 is a crucial protein that binds GTP and increases the rate of translation. [62]
HMPREF0798_01681	Cell division protein SufI	SufI is a protein responsible for cell division and is also considered a bacterial twin-arginine translocation protein [63]
HMPREF0798_01771	Mercury(II) reductase	This protein helps the organism to withstand the toxic Hg concentrations [64]

4. Conclusions

In this study, pure-grade citrate-capped CuO NP was synthesized using simple precipitation and grafting methods. From two types of copper mine tailings, CuO NPs were also extracted and functionalized with citrate. The XRD spectrum confirmed the formation of monoclinic crystals of CuO NPs with space group C2/C. FESEM and EDAX revealed the morphology of CuO NPs. The average SEM diameter of CuO NPs was around 38.1 nm, which agreed fairly well with the XRD and DLS data. FTIR and UV-vis spectroscopy confirmed the surface functionalization of the CuO NPs with the citrate ligand. The synthesized nanohybrid was found to generate ROS under UV light exposure in the DCFH assay and showed excellent antimicrobial activity against *S. hominis* bacterial strains in a triparted study consisting of growth curve analysis, agar plate assay method, and microscopic studies after staining using DAPI and PI. The C-CuO NPs were also found to possess antioxidant properties in the DPPH assay. Consequently, citrate-functionalized CuO NPs can, therefore, be used as an antibacterial agent in surface coatings, on a variety of substrates to stop microbes from adhering to them, colonizing and growing on them, and producing biofilms, such as in habitational medical equipment. This study suggests that the mechanisms of the antimicrobial response of a citrate-CuO nanohybrid in different species of bacteria should be further explored. The use of copper mine tailings as a source of raw materials for nanohybrid synthesis as a means of, simultaneously, catering low-cost antibiotics to a wider population across the globe and remediating the burden from the copper mines was also explored.

Author Contributions: A.B.: (Conceptualization: Lead; Data curation: Lead; Formal analysis: Lead; Investigation: Lead; Methodology: Lead; Project administration: Lead; Resources: Lead; Software: Lead; Validation: Lead; Visualization: Supporting; Writing—original draft: Lead; Writing—review & editing: Supporting); R.G.: (Data curation: Equal; Formal analysis: Supporting; Investigation: Supporting; Methodology: Equal; Validation: Supporting; Writing—review & editing: Supporting); T.A. (Data curation: Supporting; Formal analysis: Supporting; Validation: Supporting; Writing—review & editing: Supporting); S.M.: (Resources: Equal; Writing—review & editing: Supporting); A.C.: (Investigation: Supporting; Methodology: Supporting; Writing—review & editing: Supporting, Resources: Supporting); S.K.P.: (Conceptualization: Lead; Investigation: Supporting; Methodology: Equal; Supervision: Lead; Writing—review & editing: Supporting Formal analysis: Equal; Project

administration: Lead; Resources: Equal). All authors have read and agreed to the published version of the manuscript.

References

1. Borkow, G.; Gabbay, J. Copper, an ancient remedy returning to fight microbial, fungal and viral infections. *Curr. Chem. Biol.* **2009**, *3*, 272–278.
2. Dollwet, H. Historic uses of copper compounds in medicine. *Trace Elem. Med.* **1985**, *2*, 80–87.
3. Council, N.R. *Copper in Drinking Water*; National Academies Press: Washington, DC, USA, 2000.
4. Giannousi, K.; Sarafidis, G.; Mourdikoudis, S.; Pantazaki, A.; Dendrinou-Samara, C. Selective synthesis of Cu_2O and Cu/Cu_2O NPs: Antifungal activity to yeast Saccharomyces cerevisiae and DNA interaction. *Inorg. Chem.* **2014**, *53*, 9657–9666. [CrossRef] [PubMed]
5. Gandhare, N.V.; Chaudhary, R.G.; Meshram, V.P.; Tanna, J.A.; Lade, S.; Gharpure, M.P.; Juneja, H.D. An efficient and one-pot synthesis of 2,4,5-trisubstituted imidazole compounds catalyzed by copper nanoparticles. *J. Chin. Adv. Mater. Soc.* **2015**, *3*, 270–279. [CrossRef]
6. Tanna, J.A.; Chaudhary, R.G.; Sonkusare, V.N.; Juneja, H.D. CuO nanoparticles: Synthesis, characterization and reusable catalyst for polyhydroquinoline derivatives under ultrasonication. *J. Chin. Adv. Mater. Soc.* **2016**, *4*, 110–122. [CrossRef]
7. Sun, H.; Kim, H.; Song, S.; Jung, W. Copper foam-derived electrodes as efficient electrocatalysts for conventional and hybrid water electrolysis. *Mater. Rep. Energy* **2022**, *2*, 100092. [CrossRef]
8. Han, X.; Liu, P.; Ran, R.; Wang, W.; Zhou, W.; Shao, Z. Non-metal fluorine doping in Ruddlesden–Popper perovskite oxide enables high-efficiency photocatalytic water splitting for hydrogen production. *Mater. Today Energy* **2022**, *23*, 100896. [CrossRef]
9. Kuang, P.; Ni, Z.; Yu, J.; Low, J. New progress on MXenes-based nanocomposite photocatalysts. *Mater. Rep. Energy* **2022**, *2*, 100081. [CrossRef]
10. He, J.; Liu, P.; Ran, R.; Wang, W.; Zhou, W.; Shao, Z. Single-atom catalysts for high-efficiency photocatalytic and photoelectrochemical water splitting: Distinctive roles, unique fabrication methods and specific design strategies. *J. Mater. Chem. A* **2022**, *10*, 6835–6871. [CrossRef]
11. Ssekatawa, K.; Byarugaba, D.K.; Angwe, M.K.; Wampande, E.M.; Ejobi, F.; Nxumalo, E.; Kirabira, J.B. Phyto-Mediated Copper Oxide Nanoparticles for Antibacterial, Antioxidant and Photocatalytic Performances. *Front. Bioeng. Biotechnol.* **2022**, *10*, 820218. [CrossRef]
12. Palmer, A.; Kishony, R. Understanding, predicting and manipulating the genotypic evolution of antibiotic resistance. *Nat. Rev. Genet.* **2013**, *14*, 243–248. [CrossRef]
13. Chaudhary, R.G.; Sonkusare, V.N.; Bhusari, G.S.; Mondal, A.; Shaik, D.P.; Juneja, H.D. Microwave-mediated synthesis of spinel CuAl2O4 nanocomposites for enhanced electrochemical and catalytic performance. *Res. Chem. Intermed.* **2018**, *44*, 2039–2060. [CrossRef]
14. Kaweeteerawat, C.; Chang, C.H.; Roy, K.R.; Liu, R.; Li, R.; Toso, D.; Fischer, H.; Ivask, A.; Ji, Z.; Zink, J.I.; et al. Cu Nanoparticles Have Different Impacts in *Escherichia coli* and *Lactobacillus brevis* than Their Microsized and Ionic Analogues. *ACS Nano* **2015**, *9*, 7215–7225. [CrossRef]
15. Bogdanović, U.; Vodnik, V.; Mitrić, M.; Dimitrijević, S.; Škapin, S.D.; Žunič, V.; Budimir, M.; Stoiljković, M. Nanomaterial with High Antimicrobial Efficacy—Copper/Polyaniline Nanocomposite. *ACS Appl. Mater. Interfaces* **2015**, *7*, 1955–1966. [CrossRef] [PubMed]
16. Hsueh, Y.-H.; Tsai, P.-H.; Lin, K.-S. pH-dependent antimicrobial properties of copper oxide nanoparticles in Staphylococcus aureus. *Int. J. Mol. Sci.* **2017**, *18*, 793. [CrossRef] [PubMed]
17. Nishino, F.; Jeem, M.; Zhang, L.; Okamoto, K.; Okabe, S.; Watanabe, S. Formation of CuO nano-flowered surfaces via submerged photo-synthesis of crystallites and their antimicrobial activity. *Sci. Rep.* **2017**, *7*, 1–11. [CrossRef] [PubMed]
18. Weaver, L.; Noyce, J.; Michels, H.; Keevil, C. Potential action of copper surfaces on meticillin-resistant Staphylococcus aureus. *J. Appl. Microbiol.* **2010**, *109*, 2200–2205. [CrossRef]
19. Jadhav, S.; Gaikwad, S.; Nimse, M.; Rajbhoj, A. Copper oxide nanoparticles: Synthesis, characterization and their antibacterial activity. *J. Clust. Sci.* **2011**, *22*, 121–129. [CrossRef]
20. Pelgrift, R.Y.; Friedman, A.J. Nanotechnology as a therapeutic tool to combat microbial resistance. *Adv. Drug Deliv. Rev.* **2013**, *65*, 1803–1815. [CrossRef]
21. Zhu, Z.; Wan, S.; Zhao, Y.; Gu, Y.; Wang, Y.; Qin, Y.; Bu, Y. Recent advances in bismuth-based multimetal oxide photocatalysts for hydrogen production from water splitting: Competitiveness, challenges, and future perspectives. *Mater. Rep. Energy* **2021**, *1*, 100019. [CrossRef]

22. Xiao, H.; Liu, P.; Wang, W.; Ran, R.; Zhou, W.; Shao, Z. Enhancing the photocatalytic activity of Ruddlesden-Popper Sr2TiO4 for hydrogen evolution through synergistic silver doping and moderate reducing pretreatment. *Mater. Today Energy* **2022**, *23*, 100899. [CrossRef]

23. McDonnell, G.; Russell, A.D. Antiseptics and disinfectants: Activity, action, and resistance. *Clin. Microbiol. Rev.* **1999**, *12*, 147–179. [CrossRef]

24. Pang, H.; Gao, F.; Lu, Q. Morphology effect on antibacterial activity of cuprous oxide. *Chem. Commun.* **2009**, *9*, 1076–1078. [CrossRef] [PubMed]

25. Ren, G.; Hu, D.; Cheng, E.W.; Vargas-Reus, M.A.; Reip, P.; Allaker, R.P. Characterisation of copper oxide nanoparticles for antimicrobial applications. *Int. J. Antimicrob. Agents* **2009**, *33*, 587–590. [CrossRef] [PubMed]

26. Woźniak-Budych, M.J.; Przysiecka, Ł.; Maciejewska, B.M.; Wieczorek, D.; Staszak, K.; Jarek, M.; Jesionowski, T.; Jurga, S. Facile Synthesis of Sulfobetaine-Stabilized Cu$_2$O Nanoparticles and Their Biomedical Potential. *ACS Biomater. Sci. Eng.* **2017**, *3*, 3183–3194. [CrossRef] [PubMed]

27. Zhou, J.; Xiang, H.; Zabihi, F.; Yu, S.; Sun, B.; Zhu, M. Intriguing anti-superbug Cu$_2$O@ ZrP hybrid nanosheet with enhanced antibacterial performance and weak cytotoxicity. *Nano Res.* **2019**, *12*, 1453–1460. [CrossRef]

28. Hotze, E.M.; Phenrat, T.; Lowry, G.V. Nanoparticle Aggregation: Challenges to Understanding Transport and Reactivity in the Environment. *J. Environ. Qual.* **2010**, *39*, 1909–1924. [CrossRef]

29. Mondal, S.; Ghosh, R.; Adhikari, A.; Pal, U.; Mukherjee, D.; Biswas, P.; Darbar, S.; Singh, S.; Bose, S.; Saha-Dasgupta, T.; et al. In vitro and Microbiological Assay of Functionalized Hybrid Nanomaterials To Validate Their Efficacy in Nanotheranostics: A Combined Spectroscopic and Computational Study. *Chemmedchem* **2021**, *16*, 3739–3749. [CrossRef]

30. Zhang, L.; Thomas, J.C.; Miragaia, M.; Bouchami, O.; Chaves, F.; d'Azevedo, P.A.; Robinson, D.A. Multilocus sequence typing and further genetic characterization of the enigmatic pathogen, Staphylococcus hominis. *PLoS ONE* **2013**, *8*, e66496. [CrossRef]

31. Kim, S.-D.; McDonald, L.C.; Jarvis, W.R.; McAllister, S.K.; Jerris, R.; Carson, L.A.; Miller, J.M. Determining the Significance of Coagulase-Negative Staphylococci Isolated From Blood Cultures at a Community Hospital A Role for Species and Strain Identification. *Infect. Control. Hosp. Epidemiology* **2000**, *21*, 213–217. [CrossRef]

32. Iyer, M.N.; Wirostko, W.J.; Kim, S.H.; Simons, K.B. Staphylococcus hominis Endophthalmitis Associated With a Capsular Hypopyon. *Am. J. Ophthalmol.* **2005**, *139*, 930–932. [CrossRef]

33. Lam, T.H.; Verzotto, D.; Brahma, P.; Ng, A.H.Q.; Hu, P.; Schnell, D.; Tiesman, J.; Kong, R.; Ton, T.M.U.; Li, J.; et al. Understanding the microbial basis of body odor in pre-pubescent children and teenagers. *Microbiome* **2018**, *6*, 1–14. [CrossRef] [PubMed]

34. Zhu, J.; Li, D.; Chen, H.; Yang, X.; Lu, L.; Wang, X. Highly dispersed CuO nanoparticles prepared by a novel quick-precipitation method. *Mater. Lett.* **2004**, *58*, 3324–3327. [CrossRef]

35. Mallakpour, S.; Dinari, M.; Azadi, E. Grafting of Citric Acid as a Green Coupling Agent on the Surface of CuO Nanoparticle and its Application for Synthesis and Characterization of Novel Nanocomposites Based on Poly(amide-imide) Containing*N*-trimellitylimido-L-valine Linkage. *Polym. Technol. Eng.* **2015**, *54*, 594–602. [CrossRef]

36. Nawaz, A.; Goudarzi, S.; Asghari, M.A.; Pichiah, S.; Selopal, G.S.; Rosei, F.; Wang, Z.M.; Zarrin, H. Review of Hybrid 1D/2D Photocatalysts for Light-Harvesting Applications. *ACS Appl. Nano Mater.* **2021**, *4*, 11323–11352. [CrossRef]

37. Ahmed, S.A.; Hasan, N.; Bagchi, D.; Altass, H.M.; Morad, M.; Althagafi, I.I.; Hameed, A.M.; Sayqal, A.; Khder, A.E.R.S.; Asghar, B.H.; et al. Nano-MOFs as targeted drug delivery agents to combat antibiotic-resistant bacterial infections. *R. Soc. Open Sci.* **2020**, *7*, 200959. [CrossRef] [PubMed]

38. Tinajero-Díaz, E.; Salado-Leza, D.; Gonzalez, C.; Martínez Velázquez, M.; López, Z.; Bravo-Madrigal, J.; Hernández-Gutiérrez, R. Green metallic nanoparticles for cancer therapy: Evaluation models and cancer applications. *Pharmaceutics* **2021**, *13*, 1719. [CrossRef] [PubMed]

39. Mondal, S.; Adhikari, A.; Ghosh, R.; Singh, M.; Das, M.; Darbar, S.; Bhattacharya, S.S.; Pal, D.; Pal, S.K. Synthesis and spectroscopic characterization of a target-specific nanohybrid for redox buffering in cellular milieu. *MRS Adv.* **2021**, *6*, 427–433. [CrossRef]

40. Polley, N.; Saha, S.; Adhikari, A.; Banerjee, S.; Darbar, S.; Das, S.; Pal, S.K. Safe and symptomatic medicinal use of surface-functionalized Mn$_3$O$_4$ nanoparticles for hyperbilirubinemia treatment in mice. *Nanomedicine* **2015**, *10*, 2349–2363. [CrossRef]

41. Bera, A.; Hasan, N.; Pal, U.; Bagchi, D.; Maji, T.K.; Saha-Dasgupta, T.; Das, R.; Pal, S.K. Fabrication of nanohybrids toward improving therapeutic potential of a NIR photo-sensitizer: An optical spectroscopic and computational study. *J. Photochem. Photobiol. A Chem.* **2022**, *424*, 113610. [CrossRef]

42. Hasan, N.; Bera, A.; Maji, T.K.; Mukherjee, D.; Pan, N.; Karmakar, D.; Pal, S.K. Functionalized nano-MOF for NIR induced bacterial remediation: A combined spectroscopic and computational study. *Inorganica Chim. Acta* **2022**, *532*, 120733. [CrossRef]

43. Szklarczyk, D.; Santos, A.; Von Mering, C.; Jensen, L.J.; Bork, P.; Kuhn, M. STITCH 5: Augmenting protein–chemical interaction networks with tissue and affinity data. *Nucleic Acids Res.* **2016**, *44*, D380–D384. [CrossRef] [PubMed]

44. Kuhn, M.; Szklarczyk, D.; Pletscher-Frankild, S.; Blicher, T.H.; von Mering, C.; Jensen, L.J.; Bork, P. STITCH 4: Integration of protein–chemical interactions with user data. *Nucleic Acids Res.* **2013**, *42*, D401–D407. [CrossRef] [PubMed]

45. Wang, B.; Wu, X.-L.; Shu, C.-Y.; Guo, Y.-G.; Wang, C.-R. Synthesis of CuO/graphene nanocomposite as a high-performance anode material for lithium-ion batteries. *J. Mater. Chem.* **2010**, *20*, 10661–10664. [CrossRef]

46. Asbrink, S.; Waskowska, A. CuO: X-ray single-crystal structure determination at 196 K and room temperature. *J. Physics Condens. Matter* **1991**, *3*, 8173–8180. [CrossRef]

47. Patterson, A.L. The Scherrer Formula for X-Ray Particle Size Determination. *Phys. Rev.* **1939**, *56*, 978–982. [CrossRef]

48. Ahamed, M.; Alhadlaq, H.A.; Khan, M.A.M.; Karuppiah, P.; Al-Dhabi, N.A. Synthesis, Characterization, and Antimicrobial Activity of Copper Oxide Nanoparticles. *J. Nanomater.* **2014**, *2014*, 1–4. [CrossRef]
49. Moniri, S.; Ghoranneviss, M.; Hantehzadeh, M.R.; Asadabad, M.A. Synthesis and optical characterization of copper nanoparticles prepared by laser ablation. *Bull. Mater. Sci.* **2017**, *40*, 37–43. [CrossRef]
50. Sen, S.; Sarkar, K. Effective Biocidal and Wound Healing Cogency of Biocompatible Glutathione: Citrate-Capped Copper Oxide Nanoparticles Against Multidrug-Resistant Pathogenic Enterobacteria. *Microb. Drug Resist.* **2021**, *27*, 616–627. [CrossRef]
51. Cantu, J.M.; Ye, Y.; Valdes, C.; Cota-Ruiz, K.; Hernandez-Viezcas, J.A.; Gardea-Torresdey, J.L. Citric Acid-Functionalized CuO Nanoparticles Alter Biochemical Responses in Candyland Red Tomato (*Solanum lycopersicum*). *ACS Agric. Sci. Technol.* **2022**, *2*, 359–370. [CrossRef]
52. Pabisch, S.; Feichtenschlager, B.; Kickelbick, G.; Peterlik, H. Effect of interparticle interactions on size determination of zirconia and silica based systems–A comparison of SAXS, DLS, BET, XRD and TEM. *Chem. Phys. Lett.* **2012**, *521*, 91–97. [CrossRef] [PubMed]
53. Abboud, Y.; Saffaj, T.; Chagraoui, A.; El Bouari, A.; Brouzi, K.; Tanane, O.; Ihssane, B. Biosynthesis, characterization and antimicrobial activity of copper oxide nanoparticles (CONPs) produced using brown alga extract (Bifurcaria bifurcata). *Appl. Nanosci.* **2014**, *4*, 571–576. [CrossRef]
54. Zhang, Y.; Li, N.; Xiang, Y.; Wang, D.; Zhang, P.; Wang, Y.; Lu, S.; Xu, R.; Zhao, J. A flexible non-enzymatic glucose sensor based on copper nanoparticles anchored on laser-induced graphene. *Carbon* **2020**, *156*, 506–513. [CrossRef]
55. Adhikari, A.; Bhutani, V.K.; Mondal, S.; Das, M.; Darbar, S.; Ghosh, R.; Polley, N.; Das, A.K.; Bhattacharya, S.S.; Pal, D.; et al. Chemoprevention of bilirubin encephalopathy with a nanoceutical agent. *Pediatr. Res.* **2022**, 1–11. [CrossRef]
56. Pirilä, M.; Saouabe, M.; Ojala, S.; Rathnayake, B.; Drault, F.; Valtanen, A.; Huuhtanen, M.; Brahmi, R.; Keiski, R.L. Photocatalytic Degradation of Organic Pollutants in Wastewater. *Top. Catal.* **2015**, *58*, 1085–1099. [CrossRef]
57. Ajmal, A.; Majeed, I.; Malik, R.N.; Idriss, H.; Nadeem, M.A. Principles and mechanisms of photocatalytic dye degradation on TiO$_2$based photocatalysts: A comparative overview. *RSC Adv.* **2014**, *4*, 37003–37026. [CrossRef]
58. Sibhatu, A.K.; Weldegebrieal, G.K.; Sagadevan, S.; Tran, N.N.; Hessel, V. Photocatalytic activity of CuO nanoparticles for organic and inorganic pollutants removal in wastewater remediation. *Chemosphere* **2022**, *300*, 134623. [CrossRef]
59. Sharma, I.; Ahmad, P. Catalase: A versatile antioxidant in plants. In *Oxidative Damage to Plants*; Elsevier: Amsterdam, The Netherlands, 2014; pp. 131–148.
60. Wang, T.; Xie, X.; Liu, H.; Chen, F.; Du, J.; Wang, X.; Jiang, X.; Yu, F.; Fan, H. Pyridine nucleotide-disulphide oxidoreductase domain 2 (PYROXD2): Role in mitochondrial function. *Mitochondrion* **2019**, *47*, 114–124. [CrossRef]
61. Moran, J.F.; Sun, Z.; Sarath, G.; Arredondo-Peter, R.; James, E.K.; Becana, M.; Klucas, R.V. Molecular cloning, functional characterization, and subcellular localization of soybean nodule dihydrolipoamide reductase. *Plant Physiol.* **2002**, *128*, 300–313. [CrossRef]
62. Marzi, S.; Knight, W.; Brandi, L.; Caserta, E.; Soboleva, N.; Hill, W.E.; Gualerzi, C.O.; Lodmell, J.S. Ribosomal localization of translation initiation factor IF2. *Rna* **2003**, *9*, 958–969. [CrossRef] [PubMed]
63. Tarry, M.; Arends, S.R.; Roversi, P.; Piette, E.; Sargent, F.; Berks, B.C.; Weiss, D.S.; Lea, S.M. The Escherichia coli Cell Division Protein and Model Tat Substrate SufI (FtsP) Localizes to the Septal Ring and Has a Multicopper Oxidase-Like Structure. *J. Mol. Biol.* **2009**, *386*, 504–519. [CrossRef] [PubMed]
64. Freedman, Z.; Zhu, C.; Barkay, T. Mercury Resistance and Mercuric Reductase Activities and Expression among Chemotrophic Thermophilic Aquificae. *Appl. Environ. Microbiol.* **2012**, *78*, 6568–6575. [CrossRef] [PubMed]